Producing geothermal energy with a deep borehole heat exchanger: exergy optimization of different applications and preliminary design criteria

Alimonti C[1,*], Conti P[2], Soldo E[1]

[1]University of Rome – DICMA, Via Eudossiana 18, 00184 ROMA

[2]University of Pisa – DESTEC, Largo Lucio Lazzarino - 56122 Pisa

*Corresponding author: claudio.alimonti@uniroma1.it

Abstract

This paper aims at proposing fast and plain design tools to evaluate the best energy application for deep borehole heat exchangers, exploiting geothermal resources. Exergy efficiency has been chosen as a performance index. Five possible utilization solutions have been analyzed: district heating, adsorption cooling, ORC power production, a thermal cascade system, and combined heat and power configuration. An extensive sensitivity analysis on source characteristics and well geometry has been performed to find the design criteria that ensure the maximum exergy performance. Results show that configurations involving district heating are recommended for exclusive power production. If optimized, district heating exergy efficiency can reach values in the range 40 % - 50 % when a geothermal source at the well bottom is lower than 300 °C. For higher values, the combined heat and power production is a preferable choice, reaching an exergy efficiency of up to 60 %. Design charts are also provided to read first-attempt values of the well operative temperatures and flow rate to maximize exergy efficiency for each utilization layouts.

Keywords

geothermal energy; exergy; ORC; district heating; absorption cooling plant; deep borehole heat exchanger

Nomenclature

c	specific heat capacity	[J/kg K]
ėx	specific exergy	[kJ/kg]
$\dot{E}_x$	exergy rate	[W]
K_g	temperature gradient	[°C/100 m]
İ	exergy destruction	[W]
IQR	interquartile range	
k	convective heat transfer	[W/m2 K]
H	total length of the well	[m]
ṁ	mass flow rate	[kg/s]
N_{ppr}	pipes per row number in the cooling tower	
N_R	rows number in the cooling tower	
p	pressure	[bar, MPa]

$\dot{Q}$	total thermal power	[W]
R	thermal resistance	[mK/W]
r	radius	[mm]
T	temperature	[K or °C]
t	time	[s]
$\dot{W}$	mechanical/electrical power	[W]
w_a	frontal air velocity in the cooling tower	[m/s]
z	depth	[m]

Acronyms

ABS_CHILL	absorption chiller
CP	circulation pump
CT	cooling tower
DBHE	deep borehole heat exchanger
DH	district heating
DSH+COND	desuperheater + condenser
EER	energy efficiency ratio
EVA	evaporator
FP	ORC feeding pump
HRSG	heat recovery steam generator
HEx	heat-exchanger
ORC	organic ranking cycle
PH	preheater
P	pump
SH	superheater
T	turbine
WBHX	WellBore Heat eXchanger

Greek symbols

α	thermal diffusivity	[m^2/s]
η	efficiency	
λ	thermal conductivity	[W/m K]
ϱ	density	[kg/m^3]

Subscripts, superscripts

a	ambient state
dw	downward
f	fluid
gen	generator
II	second-law
i	inner
in	inlet

o	outer
out	outlet
ret	return
s	soil property
sup	supply
up	upward
w	water
0	reference state

1. Background

The geothermal energy is a sustainable, renewable and green energy source, but unfortunately underused. In 2018 the globally installed capacity of renewable energy sources was about 2,350.7 GW (IRENA REPORT 2019), the most percentage of which (55%) was covered by hydropower (Fig.1). The global installed capacity of geothermal energy was 13.3 GW, followed only by wave power. Considering that the estimated geothermal potential for the identified resources is 6 TW (Stefansson, 2005) it is clear why the R&D areas are focusing their efforts on finding new strategies to increase geothermal development.

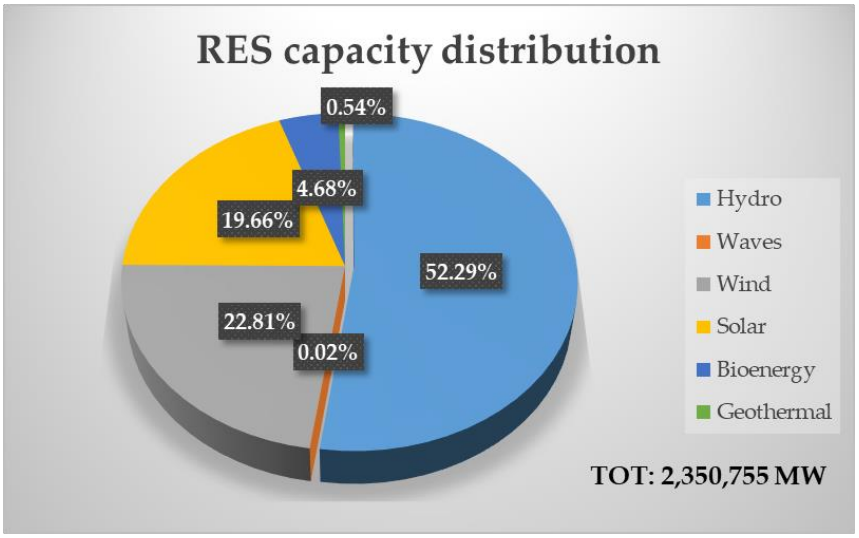

Figure 1 – Share of RES global capacity

The main obstacles to the growth of the geothermal sector are the costs and risk related to exploration and drilling phases, and the absence of social consensus among population. Gehringer and Loksha (2012) have shown that when geothermal projects reach the drilling phase, the cumulative cost is 50% of the entire project cost. An interesting solution is the use of a zero-mass extraction device, namely a deep borehole heat exchanger, which avoid all the risks (corrosion, scaling, subsidence, vapour emissions, micro-seismicity) and the treatment costs related to the extraction and reinjection of brines. The plant is a coaxial heat exchanger made of steel (Fig. 2). The heat carrier fluid is pumped in the external annulus that is separated by an insulator from the internal pipe, in which the fluid flows up to the bottomhole.

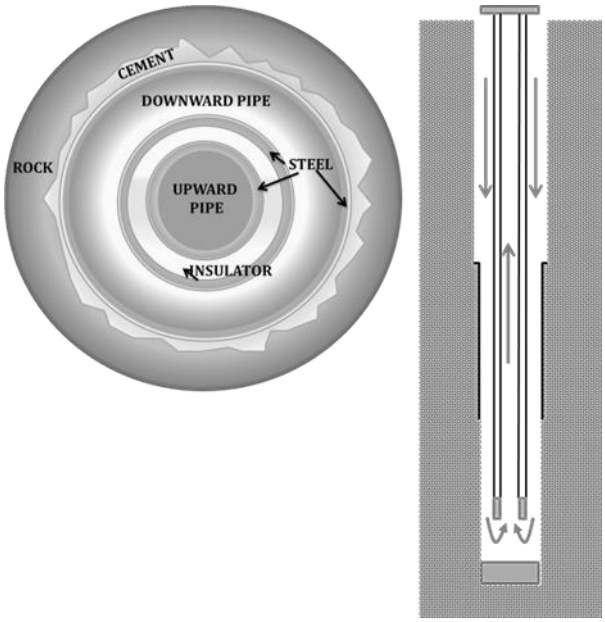

Figure 2 – The Deep Borehole Heat Exchanger.

Since 00', several authors (i.e. Kujawa et al. 2006; Wang et al. 2009; Taleghani 2013; Akhmadullin and Tyagi 2014; Mokhtari et al. 2016; Renaud et al. 2019) are studying the use of the deep borehole heat exchanger (DBHE), or WellBore Heat eXchanger (WBHX) as is named by Nalla et al. (2005), and 3 pilot tests have been realized (Kohl et al. 2002; Morita et al. 1992). The feasibility of geothermal energy production via the DBHE has been demonstrated, though the heating effectiveness of this type of closed-loop plants is much lower than conventional plants, due to the pure conductive heat extraction. Some authors consider the DBHE very promising for unexploited geothermal systems where the extraction of brines entails several issues, like volcanic ones (Galoppi et al. 2015; Alimonti et al. 2016). Furthermore, many works have proposed the use of the DBHE to repurpose depleted oil&gas wells (Alimonti and Soldo 2016; Davis and Michaelides 2009; Templeton et al. 2014; Feng et al. 2015; Noorollahi et al. 2015; Wight and Bennet, 2015), where a great amount of hot water is often present and the expensive phases of exploration, drilling and construction have already been concluded. Regarding the final use of the extracted heat, some authors have evaluated the potential electricity production via ORC plants (see Nalla et al. 2005; Wang et al. 2009; David and Michaelides 2009; Akhmadullin and Tyagi 2014; Noorollahi et al. 2015; Wight and Bennet 2015; Alimonti and Soldo 2016) whereas others of them (see Morita et al. 1992; Kohl et al. 2002; Mottaghy and Dijkshoorn 2012; Templeton et al. 2014; Le Lous et al. 2015; Caulk and Tomac 2017; Macenić and Kurevija 2018) recommend the direct use of the heat. The paper of Wang et al. (2017) illustrates a field test and the numerical investigation conducted in Xi'an, China, where the 3 DBHEs have been connected to heat pumps to provide heating and cooling for a residential area and a commercial area.

The sector of buildings air-conditioning is particularly interesting and promising for renewable energy sources and especially for geothermal energy. A study of the United Nations Environment Programme (UNEP, 2014) highlights that more than 30% of the total energy use and associated GHG emissions are produced by buildings, both in developed and developing countries. Considering that most of the worldwide heating and cooling systems are fed by natural gas or electricity produced

by fossil fuels, the geothermal energy can be strategic to reach the ambitious EU targets for 2030 and 2050 in terms of GHG cuts and RES share increase. The geothermal resources can be used to satisfy the thermal request (heat, cool, and hot water) of buildings with no GHG emissions and independently by weather conditions, thus solving also the issues related to the energy dependence of countries.

The target of this work is to identify the optimal final use for the geothermal energy produced by a deep borehole heat exchanger. Five utilization layouts have been considered in the analysis: a district heating DH plant, an absorption-chiller (ABS_CHILL) plant, a cascade system composed by a DH plant and an ABS_CHILL plant, a cascade system composed by an ORC plant and a DH plant. The four plant schemes have been applied not to a single case study but, to study the potential of the DBHE, a sensitivity analysis has been carried out, changing the ground properties, the heat exchanger parameters, the operating temperatures of the DH and the ABS_CHILL plants.

The authors consider the exergy analysis the most suitable method to evaluate a system by a thermodynamic point of view. The energy also includes a part that cannot be transformed in work, whereas the exergy is the available work. It is a measure of the maximum work output that could theoretically be obtained from a system interacting with a given environment (which is at constant pressure p_a and temperature T_a) (Di Pippo 2004; Kotas 1995). The exergy balance takes also into account the irreversible production of entropy, thus identifying both maximum theoretical performance and the inefficiencies of a system.

The geothermal literature involving the exergy is very large and it includes the classification of resources with exergy (Lee 2001; Barbacki 2012; Ramajo et al. 2010), the exergy analysis of geothermal power plants (see Di Pippo 2004; Yari 2008; Ganjehsarabi et al. 2012; Gökgedik et al. 2016; Fiaschi et al. 2017; Fallah et al. 2018) and the low enthalpy applications (ground source heat pumps, district heating and cooling, thermal storage). Ozgener et al. have analysed different geothermal DH systems in Turkey (2004, 2005, 2005) using the energy and exergy balance, thus determining the heating system performance, energy and exergy efficiencies, and exergy losses. Various articles (see Hepbasli 2005; Bi et al. 2009; Ally et al. 2015; Kang et al. 2017) are focused on the energetic and exergetic analysis of a ground source heat pump systems (GSHP) under different operating modes. For instance, this approach has been used by Hu et al. (2017) to improve the performance of a GSHP system for a public building in Wuhan, China; Erbay and Hepbasli (2014) studied a (GSHP) dryer used in food drying. Environmental and economic evaluations have been integrated with exergy analysis by some authors (i.e. Ozgener O, Hepbasli 2005; Akbulut et al. 2016). Ambrìz-Diaz et al. (2020) used advanced exergy and exergo-economic analysis for a polygeneration plant (an ORC, an absorption chiller and a dehydrator) driven by geothermal energy is the municipality of Ixtlan de Los Hervores in México. Kizilkan and Dincer (2012) have used energy and exergy analysis to evaluate a borehole thermal energy storage (BTES) plant designed to meet the cooling demand of 10 university campus buildings in Canada. Some authors used the exergy analysis for a comparison between a GSHP and an air source heat pump (ASHP) (Baccoli et al. 2015; Li et al. 2014) or between two GSHP systems (Akpinara and Hepbasli, 2007). Li et al. (2018) published

an interesting theoretical study focused on the oilfields with high water cut: the geothermal water separated is used in a polygeneration system composed by a two-stage ORC plant, an absorption chiller, the oil gathering and transport heat tracing. The authors have used energy and exergy analysis to evaluate the performance of the system. The same approach has been used by Leveni et al. (2019) to evaluate a cascade system made of an ORC and a water/lithium bromide ABS to be applied at the geothermal power plant of Torre Alfina (Italy). An integrated system combining an Organic Rankine Cycle and absorption chiller driven by geothermal energy has been investigated by Ehyaei et al. (2020) and Al-Mousawi et al. (2017).

The literature regarding the deep borehole heat exchanger reports only a few works that include a thermodynamic assessment based on exergy balance (Feng et al. 2015; Mokhtari et al. 2016; Alimonti et al. 2019): all of them analyze a DBHE connected to an Organic Rankin Cycle plant.

The present paper proposes a new approach for the sector of deep borehole heat exchangers and the final target is to produce design guidelines to identify the best application technology for a DBHE with specified conditions.

2. Methods

A homogenous performance index must be considered to properly compare different utilization strategies for DBHE technology. In this work, we refer to *exergy* concept that is widely applied in the energy sector to compare different energy forms (e.g. power and heat), systems and applications (e.g. power production, building cooling services, district heating networks) [Kotas 1005, Bejan et al 1995, Rosen&Dincer 2013]. The exergy also referred to as "availability", is a measure of the maximum work output that could theoretically be obtained from any thermodynamic system interacting with a reference environment (i.e. the dead state). Similarly, the exergy represents the minimum work that must be provided to any thermodynamic system to bring it from the dead state to a final energy state. Exergy analysis is an established methodology to investigate the quality of energy conversion processes as it can find irreversibilities and exergy losses occurring at each step and/or component [Casarosa et al 2014]. In this work, the exergy efficiency has been applied to measure the exploitation quality of a given availability of energy (i.e. geothermal source) according to the utilization scenario.

We compare the exergy performance of five reference utilization plants to be coupled with DBHE technology. The reference systems are representative of possible employment strategies for geothermal energy, namely: power production, thermal uses, cascade and/or hybrid applications. Figure 3 shows the reference layouts and the main related variables: a) district heating (DH); b) absorption cooling plant (ABS_CHILL); c) an ORC power plant; d) a cascade system composed by an ABS_CHILL cooling plant and a DH system e) a cascade system composed by an ORC power plant coupled with a DH system at the outlet section of the turbine.

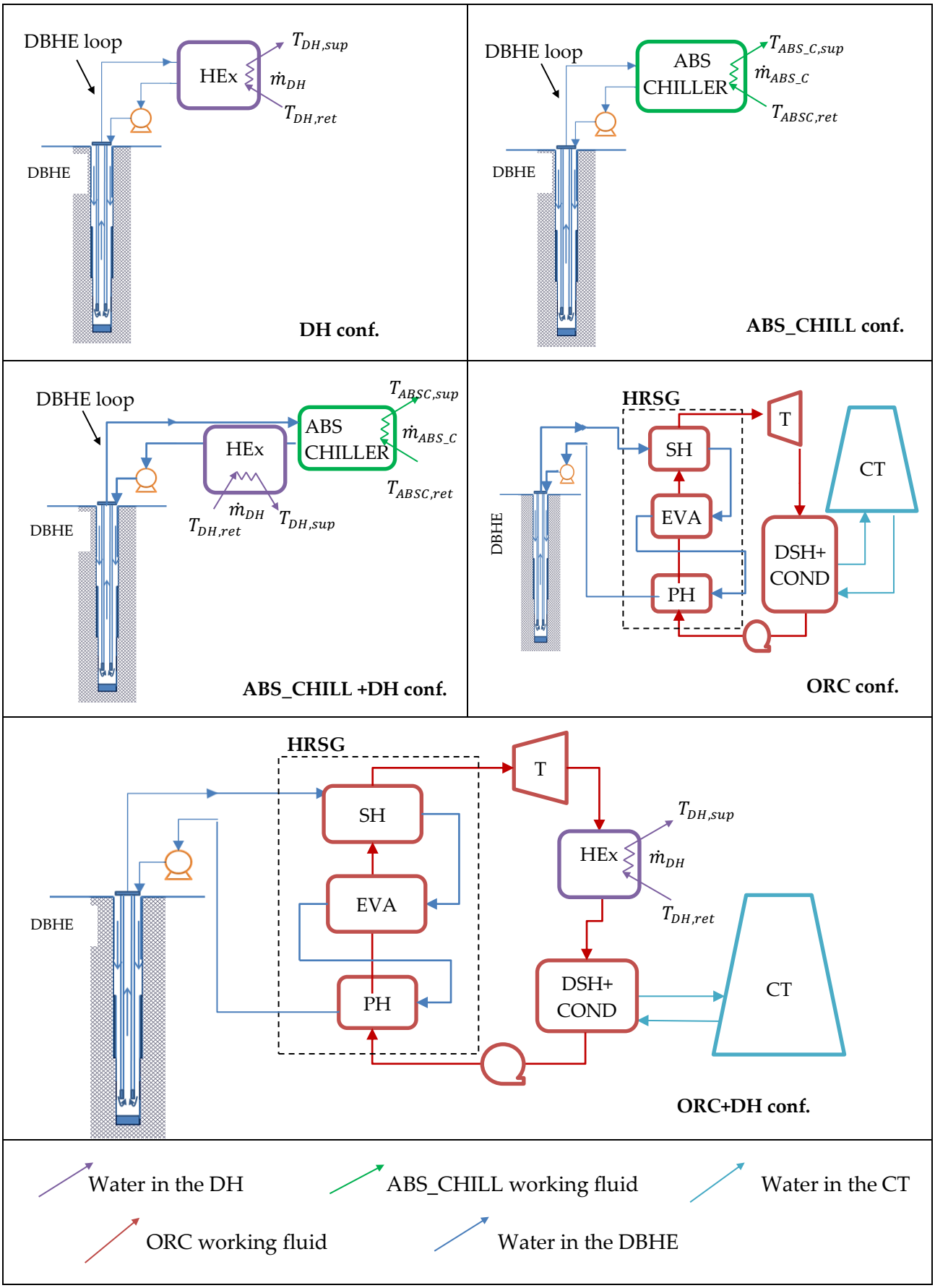

Figure 3 – Reference systems layout.

2.1. Energy and exergy models

All the components of the systems in Figure 3 are evaluated at the nominal working conditions, through steady-state mass, energy, and exergy balances, together with the overall rate equation for the heat exchangers. Thermo-physical properties of water and ORC working fluid are evaluated as a function of temperature and pressure, through the widespread software REFPROP [NIST 2013]. Table shows the values of the parameters used in this work, together with the list of unknown quantities calculated in each tested configuration. The details on components models are provided in [Alimonti et al. 2019]. Here, we recall the main modelling strategy of each component:

- Undisturbed/far-field ground temperature: the ground source is precautionary assumed as a purely conductive media. The far-field ground temperature profile is assumed as a linear function of the depth with a surface value of 25 °C (reference ambient temperature) and a constant temperature gradient over the z-direction, Kg. The values of Kg, λ_g, and α_g are objective of the next sensitivity analysis. However, their value is assumed as constant and homogeneous in all the ground source.
- DBHE: the thermal power exchanged between the circulating fluid and the far-field ground temperature is evaluated through a series of equivalent thermal resistances (Fig. 4). Axial effects are neglected, however the temperature evolution of the fluid along the WHBX ducts are evaluated through the so-called "quasi-3D approach" [Alimonti et al. 2019, Conti et al. 2016]. At a given dept, z, the following differential equation applies:

$$\begin{cases} \dot{m}_w c_w \frac{dT_{w,dw}}{dz}(z) = \frac{T_s(z)-T_{w,dw}(z)}{R_a} - \frac{T_{w,dw}(z)-T_{w,uw}(z)}{R_b} \\ -\dot{m}_w c_w \frac{dT_{w,uw}}{dz}(z) = \frac{T_{w,dw}(z)-T_{w,uw}(z)}{R_b} \end{cases} \quad (1)$$

  where R_a and R_b correspond to the resistances shown in Figure 4. R_s is the transient thermal resistance of the ground: it depends on ground thermophysical properties and the DBHE operation time [Alimonti and Soldo 2016, Conti 2016]. In this work, we refer to a year of operation as it corresponds to the period required to get sufficiently close to the steady-state value. Further details are provided in [Alimonti and Soldo 2016 and Alimonti et al. 2019]. The integration of the set of equations (1) between the inlet and outlet sections of the DBHE provides the profile of the fluid temperature over the downward and upward ducts. See Table 1 for the geometry and thermal properties of steel and insulation (air). The profile of the linear thermal power is evaluated accordingly.

  Pressure profile over the DBHE ducts is evaluated through the solution of the 1-D momentum equation over the downward and upward ducts (see Eq. 2). The z-direction is assumed as positive from the top to the bottom of the DBHE.

$$\frac{dp_{w,dw}}{dz} = g\rho_w - f_w \frac{1}{D_h}\frac{w_{f,dw}^2}{2} \quad (2)$$

  Friction coefficient, f_w, is evaluated through the classical Darcy–Weisbach equation using the Moody diagram for fully developed turbulent flows [Lavine et al. 2011]. As above-mentioned, ρ_w and f_w, are assumed as dependent from temperature and pressure, therefore "thermosiphon effect" due to density variation is included in the model, affecting the pressure drop (or increase) and the pumping energy required between DBHE inlet and outlet

sections. The pumping process in the main DBHE pump is considered as isentropic, but the electrical-mechanical efficiency of the device is set equal to 0.6.

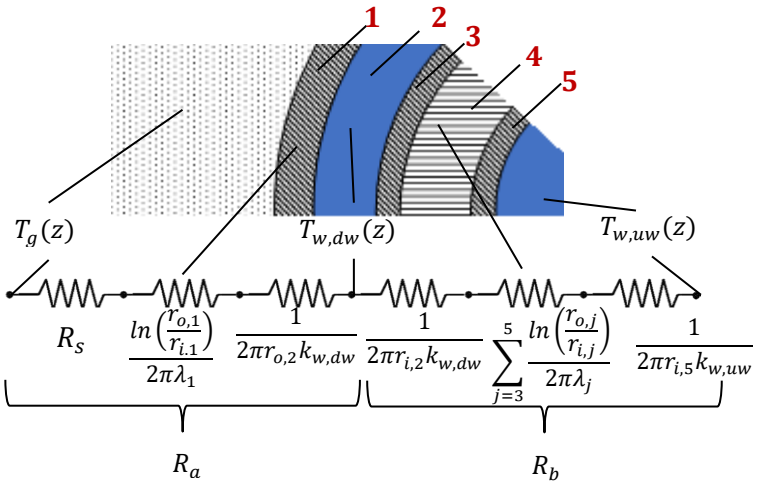

Figure 4 - DBHE thermal resistance model

Table 1- DBHE geometry and thermal properties.

Outer/Inner radius	Value
Layer 1	244.40/226.60
Layer 2	226.60/177.8
Layer 3	177.8/150.36
Layer 4	150.36/88.90
Layer 5	88.90/77.92
Thermal conductivity: $\lambda_1, \lambda_3, \lambda_5$	50 $W/(mK)$
Thermal conductivity λ_4	0.04 $W/(mK)$

- District heating: the district heating network is modelled as water flow to be heated from 60 °C to 90 °C. The useful flow rate, $\dot{m}_{DH}$, and the corresponding thermal power are calculated considering a heat transfer effectiveness of the main DH heat exchanger equal to 0.8.
- Absorption chiller: the end-user chiller loop works with supply and returns temperatures of 7 °C and 12 °C, respectively. The chiller is assumed as an indirect-fired unit, namely the generator is equipped with a heat exchanger that allows the energy transfer between the hot water from the DBHE loop and the refrigerant mixture (e.g., LiBr-H_2O). The temperature required at the generator, $T_{ABS\_CHILL,gen}$, is assumed equal to 100 °C. The heat exchanger within the ABS_CHILL generator is assumed to be sufficiently long to ensure a unitary heat transfer effectiveness: in other words, the DBHE fluid leaves the absorption unit with a temperature, T_{w,out,ABS_CHILL}, equal to the one required in the ABS_CHILL generator. The performance of the chiller is evaluated through the Second-Law thermal efficiency method, according to sources temperatures and exergy efficiency, $\eta^{II}_{ABS\_CHILL}$, assumed as constant and equal to 0.3.

$$EER = \eta^{II}_{ABS\_CHILL}\left[\frac{\frac{1}{T_a}-\frac{1}{T_{ABS\_CILL,gen}}}{\frac{1}{T_{ABS\_CHILL,sup}}-\frac{1}{T_a}}\right] \quad (3)$$

- ORC power plant and cooling tower: following the results presented in [Alimonti et al. 2019], the considered working fluid is 2-methylpropane (isobutane). Depending on the temperature at the DBHE outlet section, the power of the Hirn cycle is calculated assuming condenser temperature, pinch point and approach value of all the heat exchangers; isentropic and electrical-mechanical efficiency of the turbine and feeding pump. As above-mentioned, all these assumed values are shown in Table 2. The power required by the fans in the cooling tower is evaluated according to the model presented in the Appendix of [Alimonti et al. 2019]. For each tested configuration, the geometry of the finned surface (i.e., number of rows, N_R, and the number of ducts per row, N_{ppr}) and the frontal air velocity, w_a, are optimized

through a genetic algorithm to minimize electricity input, ensuring the required heat exchange at the condenser.

The considered expressions of the exergy efficiency for each configuration is the following:

$$\eta_{DH}^{II} = \frac{\dot{m}_{DH}(ex_{DH,sup} - ex_{DH,ret})}{Ex_{DBHE}^{\dot{Q}} + \dot{W}_{P,DBHE}} \quad (4)$$

$$\eta_{ABS\_CHILL}^{II} = \frac{\dot{m}_{ABS\_CHILL}(ex_{ABS\_CHILL,sup} - ex_{ABS\_CHILL,ret})}{Ex_{DBHE}^{\dot{Q}} + \dot{W}_{P,DBHE}} \quad (5)$$

$$\eta_{ABS\_CHILL+DH}^{II} = \frac{\dot{m}_{DH}(ex_{DH,sup} - ex_{DH,ret}) + \dot{m}_{ABS\_CHILL}(ex_{ABS\_CHILL,sup} - ex_{ABS\_CHILL,ret})}{Ex_{DBHE}^{\dot{Q}} + \dot{W}_{P,DBHE}} \quad (6)$$

$$\eta_{ORC}^{II} = \frac{\dot{W}_{ORC,net} - \dot{W}_{P,DBHE} - \dot{W}_{CT}}{Ex_{DBHE}^{\dot{Q}}} \quad (7)$$

$$\eta_{ORC+DH}^{II} = \frac{\dot{m}_{DH}(ex_{DH,sup} - ex_{DH,ret}) + \dot{W}_{ORC,net} - \dot{W}_{P,DBHE} - \dot{W}_{CT}}{Ex_{DBHE}^{\dot{Q}}} \quad (8)$$

where ex is the physical exergy associated with the fluid stream $\dot{m}$, and $Ex_{DBHE}^{\dot{Q}}$ is the exergy associated to the heat flow between the undisturbed ground and the DBHE circulating fluid. $\dot{W}$ is input or output electrical power or exergy. The reference environmental state is $T_a = 25\ °C$ and $p_a = 1\ bar$.

Table 2. Assumed parameters and unknows for each configuration,

Parameter	**Value**	**Quantities to be determined in each configuration**
District Heating (confs. DH, ABS_CHILL+DH, ORC+DH)		
Supply temperature, $T_{DH,sup}$	90 °C	$\dot{m}_{DH}$, $\dot{Q}_{DH}$, $T_{w,out,HEx}$, $T_{w,in,DBHE}$, $T_{w,out,DBHE}$, $p_{w,in,DBHE}$, $p_{w,out,DBHE}$, $\dot{W}_{P,DBHX}$
Return temperature, $T_{DH,ret}$	60 °C	
Heat exchanger effectiveness, ϵ_{HEx}	0.8	
Absorption Chiller (confs. ABS_CHILL, ABS_CHILL+DH)		
Generation temperature, $T_{ABS\_CHILL,gen}$	100 °C	$\dot{m}_{ABS\_C}$, $\dot{Q}_{ABS\_CHILL}$, T_{w,out,ABS_C}, $T_{w,in,DBHE}$, $T_{w,out,DBHE}$, $p_{w,in,DBHE}$, $p_{w,out,DBHE}$, $\dot{W}_{P,DBHX}$
Outlet temperature of the DBHX loop from the generator	100 °C	
Second-Law efficiency	0.3	
Supply temperature, $T_{ABS\_CHILL,sup}$	7 °C	
Return temperature, $T_{ABS\_CHILL,ret}$	12 °C	
ORC power plant (confs. ORC, ORC+DH)		
Working fluid	2-methylpropane (Isobutane)	$\dot{m}_{wf}$, p_{EVA}, $\dot{W}_T$, $\dot{W}_{FP}$, $T_{w,out,HRSG}$, N_{ppr}, N_R, w_a, $T_{w,in,DBHE}$,
HRSG pinch point	5 K	

HRSG approach	10 K	$T_{w,out,DBHE}$, $p_{w,in,DBHE}$, $p_{w,out,DBHE}$, $\dot{W}_{P,DBHX}$
Turbine isentropic efficiency	0.85	
Turbine electro-mechanical efficiency	0.95	
Condensing pressure	5.5 bar	
Condensing temperature	41.3 °C	
Condenser pinch point	5 K	
Feeding pump electrical-mechanical efficiency	0.6	
Cooling tower		
Approach point	5 K	
Air temperature variation	10 K	
Fans electrical-mechanical efficiency	0.6	
Fin width	5×10^{-4} m	
Fin spacing	5×10^{-3} m	
Space between two rows	0.05 m	
Space between two consecutive pipes the same row	0.05 m	
Coil inner/outer diameter	$18/22 \times 10^{-3}$ m	

3. Sensitivity analysis and optimization of the exergy performances

This work presents a sensitivity analysis of the exergy efficiency indexes (see Equations 4 – 8) depending on the characteristics of the ground source and DBHE geometry. The following parameters and ranges have been considered:

- Thermal diffusivity of the ground: $\alpha_g = \{10^{-7}; 5 \times 10^{-7}; 10^{-6}\}$ m²/s
- Thermal conductivity of the ground source: $\lambda_g = \{1; 2; 3\}$ W/(m K)
- Ground temperature gradient, $K_g = \{30; 60; 90; 120; 150\}$ K/km
- DBHE depth, $H = \{1,2,3,4,5\}$ km

Globally, we tested 225 different configurations for each of the 5 layouts in Figure 3. For each one of the tested configurations, the energy and the exergy balance of each component are evaluated through an in-house MATLAB® code.

According to the assumptions and the modelling strategy illustrated in Section 2, the DH, ABS_CHILL, and ABS_CHILL+DH configurations have a single degree of freedom corresponding to the DBHE flow rate, $\dot{m}_{w,DBHE}$. In other words, for given values of α_g, λ_g, K_g, and H, the solution of the energy and the exergy balance only depends on $\dot{m}_{w,DBHE}$, which becomes the actual design variable. Similarly, for ORC and ORC+DH configurations, we have two design variables: the DBHE flow rate, $\dot{m}_{w,DBHE}$, and the inlet temperature, $T_{w,in,DBHE}$. The latter values determine the evaporation pressure and the flow rate of the ORC working fluid, together with all the other quantities. The following ranges have been considered:

- DBHE flow rate: $\dot{m}_{w,DBHE} = \{1; 2 \dots 4.5; 5\} kg/s$
- DBHE inlet temperature, $T_{w,in,DBHE} = \{60; 65 \dots \min[100, T_g(H)\}$ °C

The upper limit of $T_{w,in,DBHE}$ is related to the ground temperature at the bottom of the DBHE to ensure the heating up of the circulating fluid. Globally, 37,800 simulations have been run. Not all the tested configurations are suitable for all the application strategies. To be included in the results, the following constraints must be met:

- The DBHE fluid must be at the liquid state. Proper work pressure, $p_{w,in,DBHE}$, is evaluated or each configuration through Equation 2 as a function of the fluid temperature profile within the DBHE.
- The ground temperature at the well bottom must be higher than 100 °C;
- Configurations resulting in negative exergy efficiency are discarded (e.g. the auxiliary energy consumption for pumping energy and cooling fans exceeds power production)

4. Results and discussion

In the following section, we present and discuss the results of the 15,811 simulations that are coherent with the above-mentioned constraints. Next, we focus on the 651 configurations that correspond to values of the $\dot{m}_{w,DBHE}$ and $T_{w,in,DBHE}$ that maximize the exergy efficiency for given values of α_g, λ_g, K_g, and H in the 5 layouts.

4.1. Complete view of all simulations results

Figure 5 illustrates the relation between the bottom temperature of the geothermal resource, $T_g(H)$, and the exergy efficiency. $T_g(H)$ has been chosen as the main driver variable because the temperature profile along well depth is the typical data on which operators base their decision on the best application of a geothermal source. We explored a temperature range between 100 °C and 900 °C: obviously, temperature above 400 °C is ideal and only tailored to understand the theoretical potential of the DBHX technology. In the next Section 4.2, we discuss design maps and criteria for source temperature in the range 100 ÷ 400 °C: this temperature range is more realistic for geothermal applications and especially for borehole heat exchanger devices.

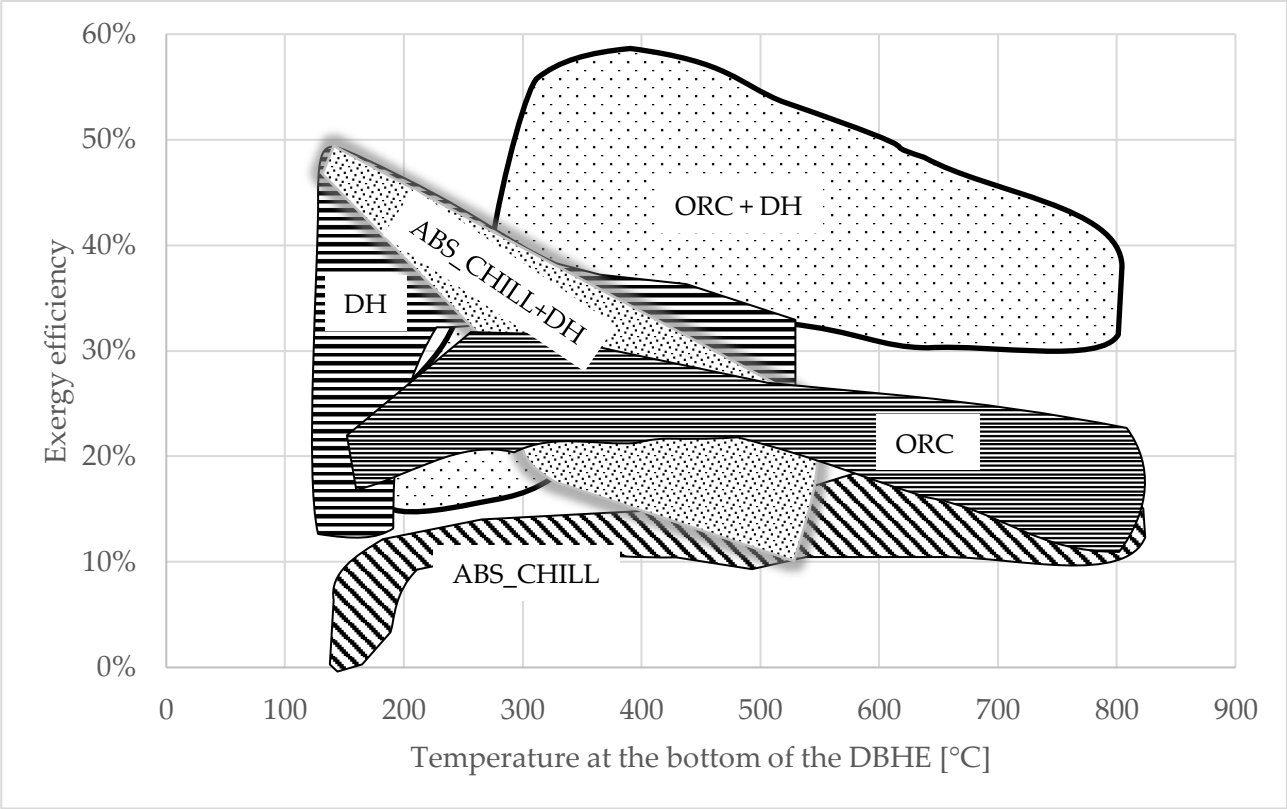

Figure 5 – Exergy efficiency versus the bottom temperature of the resource for the five layouts.

The results indicate that the ABS_CHILL configuration is the one with the lowest values of exergy efficiency (maximum about 20 %) that increases only when source temperature is between 130 °C and 200°C. For higher values of $T_g(H)$, exergy efficiency lies between 0.1 and 0.2. The region related to the ORC configuration lies in the range 20 % ÷ 30 %. For the DH configuration, the maximum exergy efficiency values are in the range 40 % ÷ 50%, but η_{DH}^{II} decreases at high source temperatures. When $T_g(H)$ is greater than 600 °C, DH and ABS_CHILL + DH technologies do not comply with the constraints of the present analysis. The presence of a DH plant in the cascade layouts produces an impressive positive effect, by doubling the upper limits of exergy efficiency for the exclusive ORC and ABS_CHILL solution.

The great number of data produces a dispersion of the results: this phenomenon is probably explained with the selection of a great number of ground and operation parameters (e.g. DBHE flow rate), some of which are not so promising for the DBHE or the user plant. For instance, when the resource temperature is 400 °C, the exergy efficiency is between 15 % and 30 % if we use an ABS_CHILL + DH solution and between 35 % and 55 % if an ORC+ DH configuration is selected. The dispersion of the results is also observed for the produced heat, power, and the irreversibility rate (see Figures 6 and 7). However, some trends can be seen and discussed.

Figure 5 can be used for preliminary screening of the most proper application for a given geothermal source condition: for $T_g(H)$: in the range 100 ÷ 300 °C, the utilization plants that include the district heating applications guarantee the higher values of exergy efficiency. In particular, the thermal-cascade ABS_CHILL + DH layout is recommended. The ORC + DH solution reaches the best exergy

performance when the temperature exceeds 300 °C. The ORC plant and the ABS_CHILL plant are the lower efficient solutions. We recall that Figure 5 only allows the selection of the most proper utilization technology from an exergy perspective; an industrial decision should include other technical, economical, regulatory, environmental elements in any specific context.

Figures 6 shows the direct correlation between source temperature and extracted heat, $\dot{Q}_{DBHE}$. The maximum value of heat extracted by the DBHE is more than 10 MW when the temperature of the geothermal resource is 775 °C. As above-mentioned, this condition is ideal and useful to understand the theoretical potential of the deep borehole heat exchangers. For a realistic range of the ground temperature, i.e. between 150 °C and 400 °C, the extracted heat is in the range 0.1 ÷2 MW per well, which makes the technology of the DBHE promising for direct uses (DH, ABS_CHILL+ DH). Under the chosen sources temperature, the ABS_CHILL has a coefficient of performance of about 1, therefore $\dot{Q}_{DBHE} \approx \dot{Q}_{ABS\_CHILL}$. ABS_CHILL+DH configuration show more constant profiles as a function of $T_g(H)$: these results depend on the assumed constraints on $T_{ABS\_CHILL,gen}$ and ϵ_{mHEx} that limit the variability of DBHE working conditions. It can be seen that $\dot{Q}_{DBHE}$ is almost halved between "hot" and "cold" useful energy. Regarding power productions, the first-law conversion efficiency of the ORC plants is in the range of 5 ÷ 10%, therefore the range of the net produced power goes from 50 to 500 kW. The use of downstream DH section does not reduce the power output, but it ensures the same amount of thermal energy. In other words, the low-temperature heat that was discharged in the ORC configuration is converted in useful exergy, increasing the overall efficiency.

Figure 6– Extracted heat, thermal power and network versus source temperature for the five layouts.

Concerning the exergy balance in the five layouts (see Figures 7), the maximum producible exergy, $\dot{E}x_{Q_g}$, increases with the temperature of the resource, anyway also the irreversibility values are growing. For instance, when the temperature of 775 °C is used in an ORC + DH layout, the maximum value of the exergy produced by the DBHE is 3.76 MW and the irreversibility is 1.06 MW; the total irreversibility is 3.08 MW. When the temperature of the resource is 175 °C, a minimum value of

about 110 kW is observed: the irreversibility produced by the deep borehole heat exchanger is 0.03 kW and the total irreversibility is 0.05 kW. The results in Figure 7 confirm what is observed in Figure 6, that is the higher the source temperature, the wider the range of exergy and irreversibility values that can be obtained by changing the operating parameters.

An inverse relation is observed between the source temperature and the exergy efficiency of DH and ABS_CHILL + DH layout: this trend can be ascribed to the deviation between the increasing exergy of the source and the fixed temperatures of the user applications. Indeed, Figures 7 shows the increasing relevance of $\dot{I}_{user}$ at high source temperatures. $\dot{I}_{ABS\_CHILL}$ values and shares indicate that the absorption chiller is the main exergy losses, even if it is working at favourable condensing temperature (25 °C). As shown in Figure 5, this DH and ABS_CHILL + DH layouts are recommended when the geothermal resource is between 150 °C and 300 °C. When the bottomhole temperature is greater than 300 °C, the ORC + DH plant can reach maximum exergy efficiency values in the range 35% ÷ 50%.

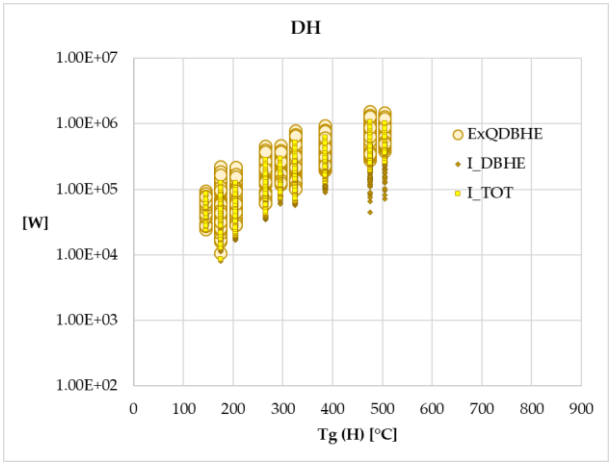

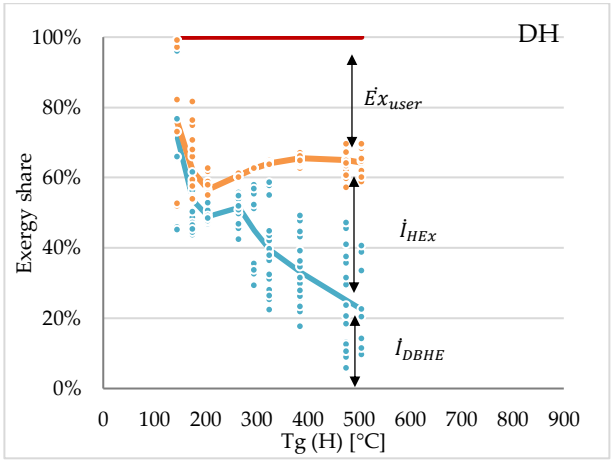

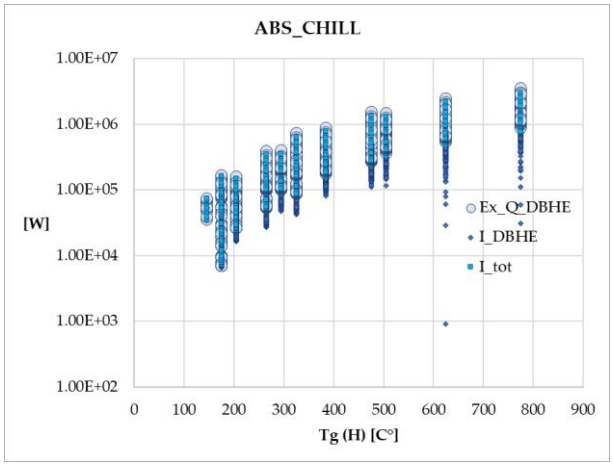

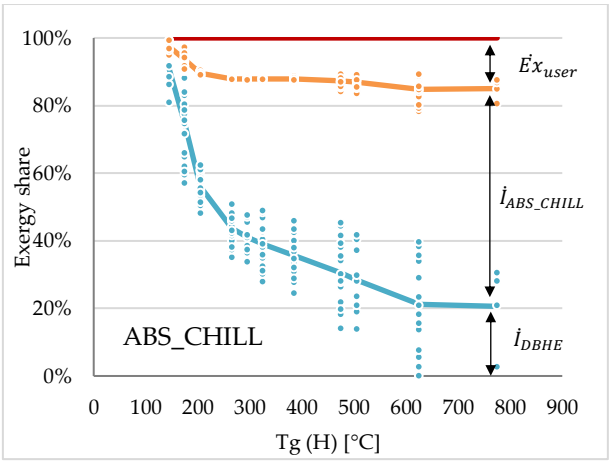

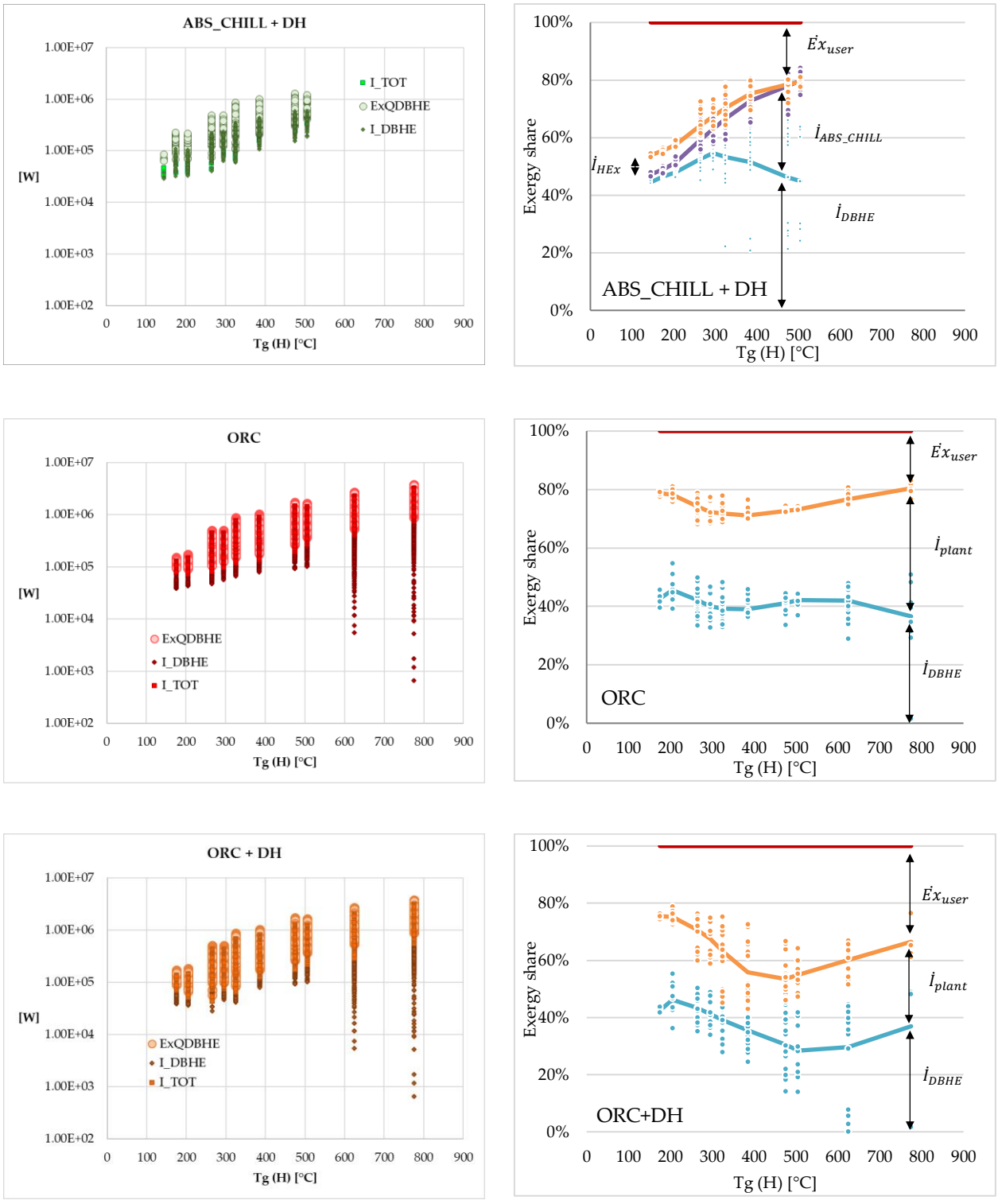

Figure 7– Produced exergy and irreversibilities versus source temperature for the five layouts.

4.2. Maximum exergy efficiency configurations

This section illustrates the results and design guidelines regarding the configurations with optimized exergy efficiency. Figure 8 shows the maximum value of η^{II} obtained for each combination of α_g, λ_g, K_g, and H, corresponding to the optimal value of $\dot{m}_{w,DBHE}$ and $T_{w,in,DBHE}$. The results are shown in Figure 8 confirm thermal uses (i.e., DH and ABS_CHILL+DH configurations)

as the optimal choice for geothermal sources up to 300 °C. For higher ground temperatures, the configuration ORC+DH shows the highest exergy efficiency.

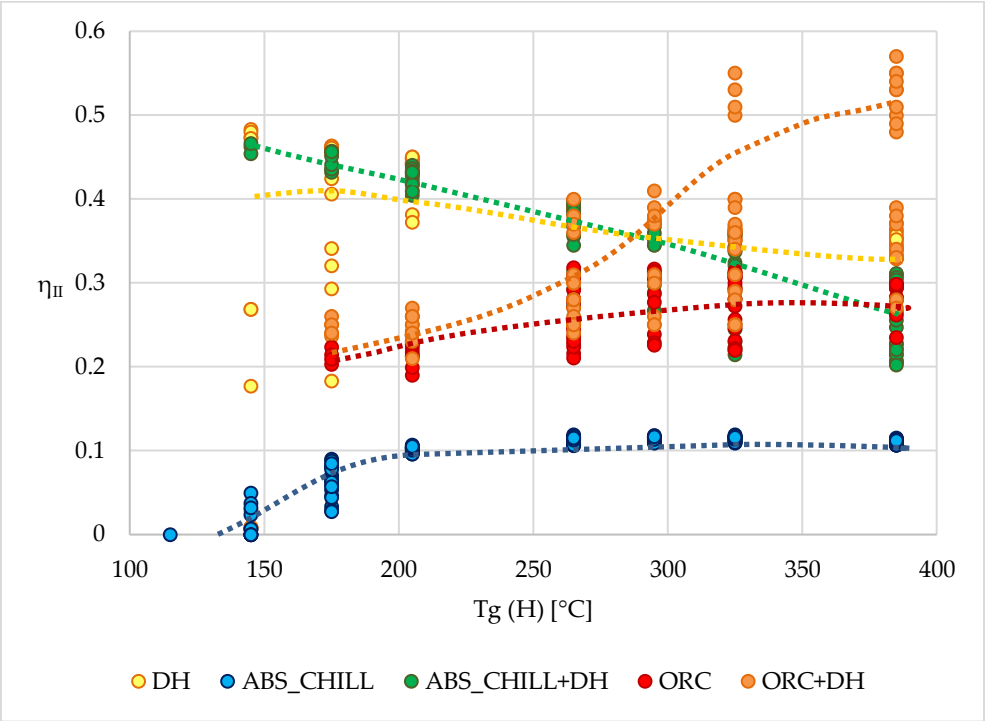

Figure 8 – Bottomhole temperature vs exergy efficiency for the configurations with maximum η^{II}.

Figures 9 – 13 show the values of the main design variables for each application layout to achieve the maximum exergy efficiency. As described in Section 3, the design variables to be optimized are:

- The DBHE flow rate, $\dot{m}_{w,DBHE}$, for DH, ABS_CHILL, and ABS_CHILL+DH configurations;
- The DBHE flow rate, $\dot{m}_{w,DBHE}$ and the inlet temperature, $T_{w,in,DBHE}$, for ORC and ORC+DH configurations.

As above-mentioned, a tailored design and optimization procedures must be performed in any specific context or project; however, Figures 9 – 13 can be used as preliminary design maps, first-attempt values, or to obtain information on the optimal tends of design variables.

DH applications

The DH configuration consists of two heat exchangers in series (see Figure 3). As well-known from exergy theory [Bejan et al 1995], the Number of Transfer Units (NTU) and the temperature profiles of the heat exchanging media is the main drivers that determine the entropy generation in a heat exchanger. In the DH configuration, we have three main heat exchanging media: the ground temperature profile, the DBHE loop and the DH loop. The analysis of the 135 solutions corresponding to the maximum exergy efficiency showed of three dimensionless numbers: RT_{DH}, NTU_{DBHE} and RT_{DBHE}, defined as:

$$RT_{DBHE} = \frac{T_{w,out,DBHE} - T_{w,in,DBHE}}{T_g(H) - T_{w,in,DBHE}} \qquad NTU_{DBHE} = \frac{H}{R_a \, \dot{m}_{DBHE} \, \overline{c_{w,dw,DBHE}}} \qquad RT_{DH} = \frac{T_{w,in,DBHE} - T_{DH,ret}}{T_g(H) - T_{DH,ret}}$$

Figure 9-a shows the distribution of RT_{DH} values for the DH configurations with the maximum η_{DH}^{II} value. The IQR is focused around 0.1 that can be used to estimate the optimal $T_{w,in,DBHE}$ as a function of the DH loop and geothermal source temperature. Alternatively, 0.08 and 0.15 are suggested for high and low values of $T_g(H)$, respectively. Figure 9-b shows the relationship between the optimal values of RT_{DBHE} and NTU_{DBHE}: it can be used to determine the optimal $\dot{m}_{DBHE}$ as a function of the DBHE and ground source characteristics once that the temperature variation $T_{w,in,DBHE} - T_{w,out,DBHE}$ has been determined according to the mHEx heat transfer effectiveness, DH loop capacity and operative temperatures.

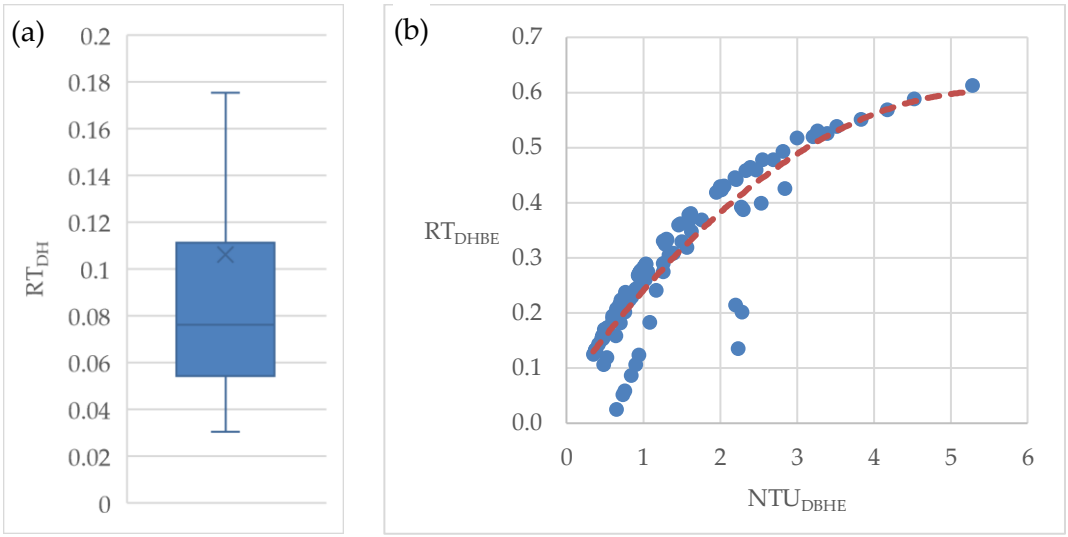

Figure 9 – Dimensionless groups for the maximum-exergy design variables of DH utilization systems: (a) box and whisker plot of RT_{DH}; (b) optimal RT_{DBHE} as a function of optimal NTU_{DBHE}.

ABS_CHILL

Figures 10 show the distribution of the optimal value of the DBHE inlet temperature and flow rate. for the ABS_CHILL configuration. The optimal values are concentrated on a single value. The inlet temperature, $T_{w,in,DBHE}$, for the ABS_CHILL always corresponds to the generation temperature of the absorption device (i.e., 100 °C for the present analysis) and it is not an actual design value. This conclusion derives to the high values of the heat transfer effectiveness between the DBHE loop and the refrigerant mixture. The optimal DBHE flow rate $\dot{m}_{w,DBHE}$ corresponds to the minimum feasible value as this condition reduce the mean temperature difference between the ground source and the circulating fluid and the irreversibility rate $\dot{I}_{DBHE}$.

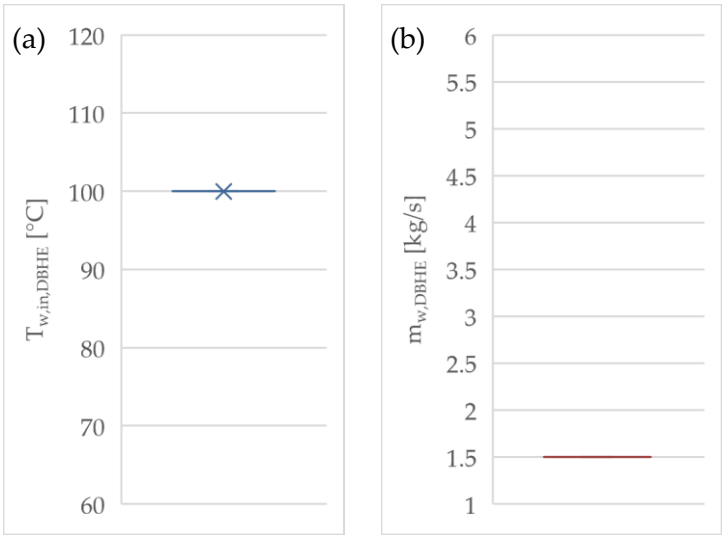

Figure 10 – Maximum-exergy design variables for ABS_CHILL utilization system: (a) DBHE inlet temperature; (b) DBHE flow rate.

ABS_CHILL+DH

Figures 11 show the distribution of the optimal value of the DBHE inlet temperature and flow rate for ABS_CHILL+DH configuration. The optimal values of $T_{w,in,DBHE}$ is a single value, i.e., 68 °C. This value depends on the assumption of $T_{ABS\_CILL,gen}$ and ϵ_{mHEx} and it is not an actual design variable. There is not a single value of the optimal DBHE flow rate, but it depends on the ground source characteristics. Apart from some outliers, there is a good correlation between $T_g(H)$ and the dimensionless group NTU_{DBHE}. In other words, the design maps in Figure 11 allows the estimation of the optimal DBHE flow rate, $\dot{m}_{w,DBHE}$, as a function of geometry and thermophysical properties (i.e., H and, R_a).

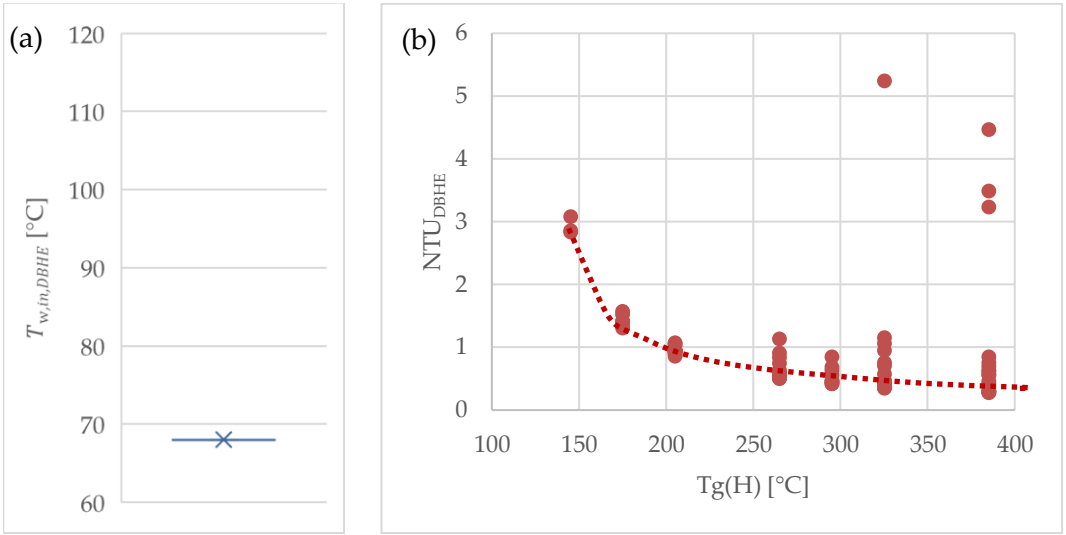

Figure 11 – Dimensionless groups for the maximum-exergy design variables of DH utilization systems: (a) DBHE inlet temperature; (b) optimal NTU_{DBHE} as a function of bottomhole temperature, $T_g(H)$.

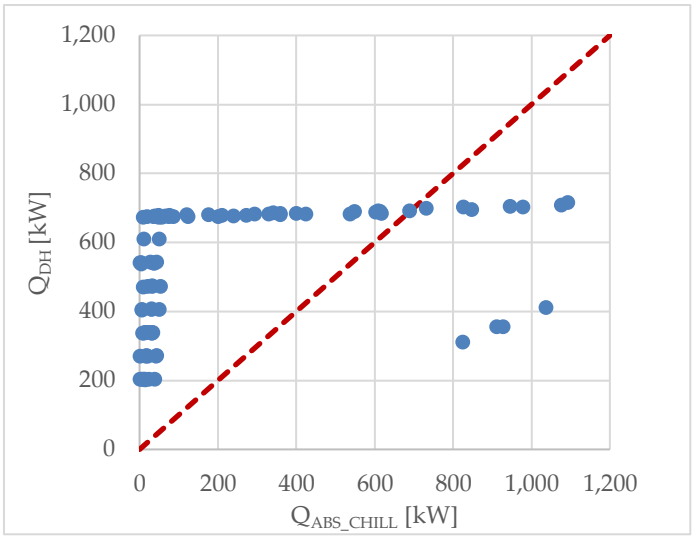

Figure 12 – Useful "hot" and "cold" heat delivered by the ABS_CHILL + DH utilization system in the optimal exergy configuration.

Additionally, Figure 12 shows the DH and the ABS_CHILL useful thermal power delivered in the optimal exergy configuration. We note that the $\dot{Q}_{DH}$ is greater than $\dot{Q}_{ABS\_CHILL}$ for almost all the cases. We conclude that DH is a more efficient use for the energy extracted by the DBHE, for the absorption technology.

ORC

Figures 13 show the distribution of the optimal value of the DBHE inlet temperature and flow rate for the ORC configuration. In the case of exclusive power production, the best design strategy is the one that maximizes the temperature level of the HRSG and the exergy efficiency of the power cycle. The distribution of the optimal $T_{w,in,DBHE}$ values are concentrated on the upper boundary of tested ranges (i.e., about $\approx 100\ °C$). Similarly, the best value for the DBHE flow rate corresponds to the lower boundary (i.e. $\approx 1.5\ kg/s$) to maximize the DBHE outlet temperature. p_{EVA} it is not an actual design value, as its value depends on the assumptions on the HRSG approach and pinch point. However, the p_{EVA} distribution in the optimal configurations is concentrated on the upper limit of the working fluid, resulting in high evaporation temperatures. All these elements lead to the conclusion that the ORC power cycle has a predominant role as irreversibility source for the DBHE.

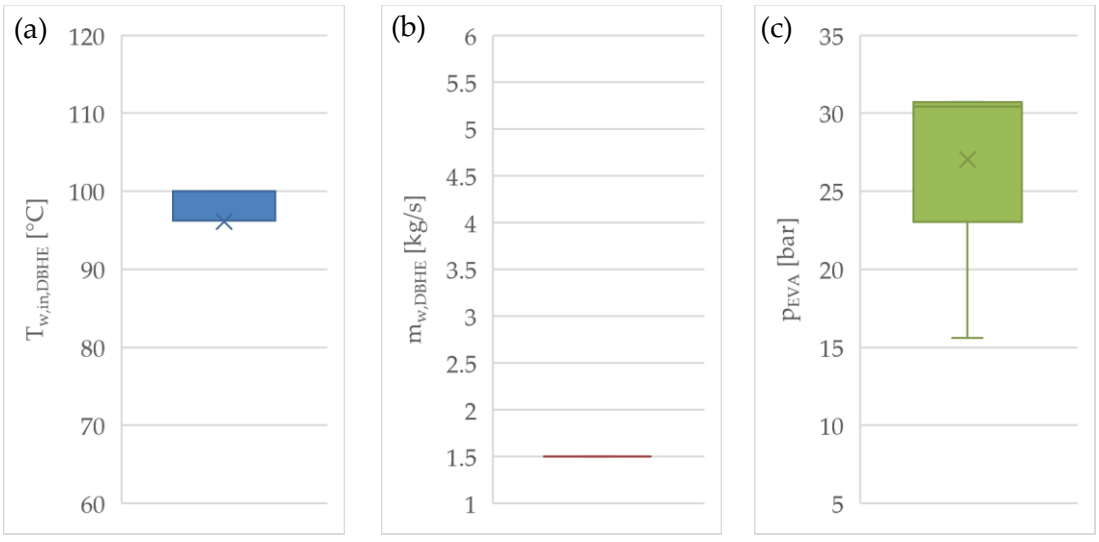

Figure 13 – Maximum-exergy design variables for ORC utilization system: (a) DBHE inlet temperature; (b) DBHE flow rate; (c) evaporation pressure.

ORC+DH

As above-mentioned, the downstream DH section does not alter the operational characteristics of the DBHE and ORC cycle, but it reduces the irreversibility generation in the DH+COND section of the power plant. Therefore, also in the ORC+DH configuration, the best values of $T_{w,in,DBHE}$ and $\dot{m}_{w,DBHE}$ are the ones that increase the temperature level of the HRSG, namely $T_{w,in,DBHE} \approx 100\ °C$ and $\dot{m}_{w,DBHE} \approx 1{,}5\ kg/s$ (see Figures 14).

As for the combined configuration ABS_CHILL+DH, it is possible to analyze which form of user-product should be preferred, Figure 15-a shows the power and thermal production of the ORC+DH configurations with the maximum exergy efficiency. We note that some points are associated with greater power production, while others are in favour of thermal one. This result can result as contradictory concerning the maximization of the ORC efficiency. However, the explanation can be inferred from Figure 15-b which shows the optimal ratio between power and heat production as a function of $T_{w,DBHE,out}$.. At a given $T_{w,DBHE,out}$ the de-superheating section of the cycle exceeds the power production due to the constraint on the evaporation pressure. The threshold value ($\approx 170°C$ in this analysis) depends on the critical pressure of the working fluid and approach value of the HRSG. Other fluids and power cycles should be employed at higher source temperature, however, the positive effects of the downstream DH section are confirmed.

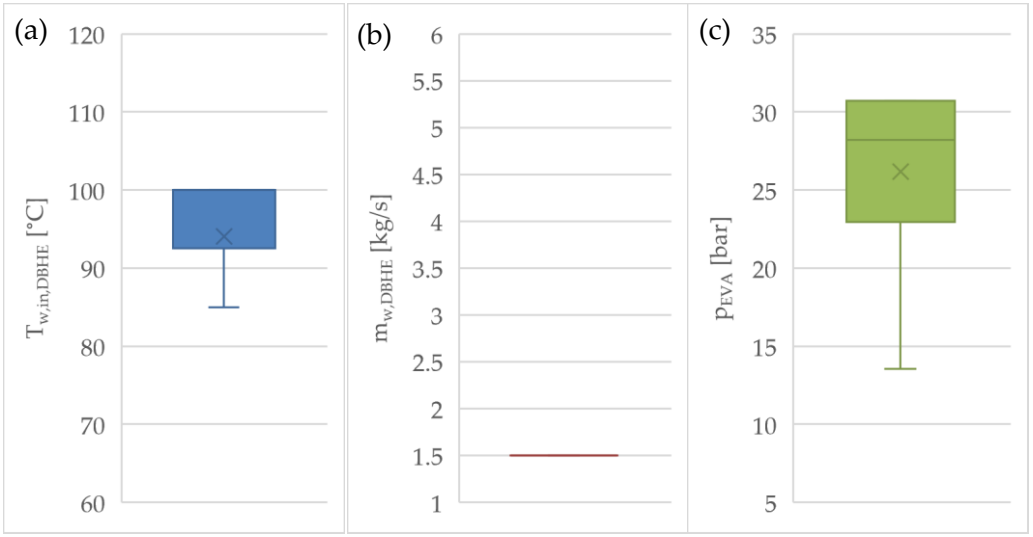

Figure 14 – Maximum-exergy design variables for ORC+DH utilization system: (a) DBHE inlet temperature; (b) DBHE flow rate; (c) evaporation pressure..

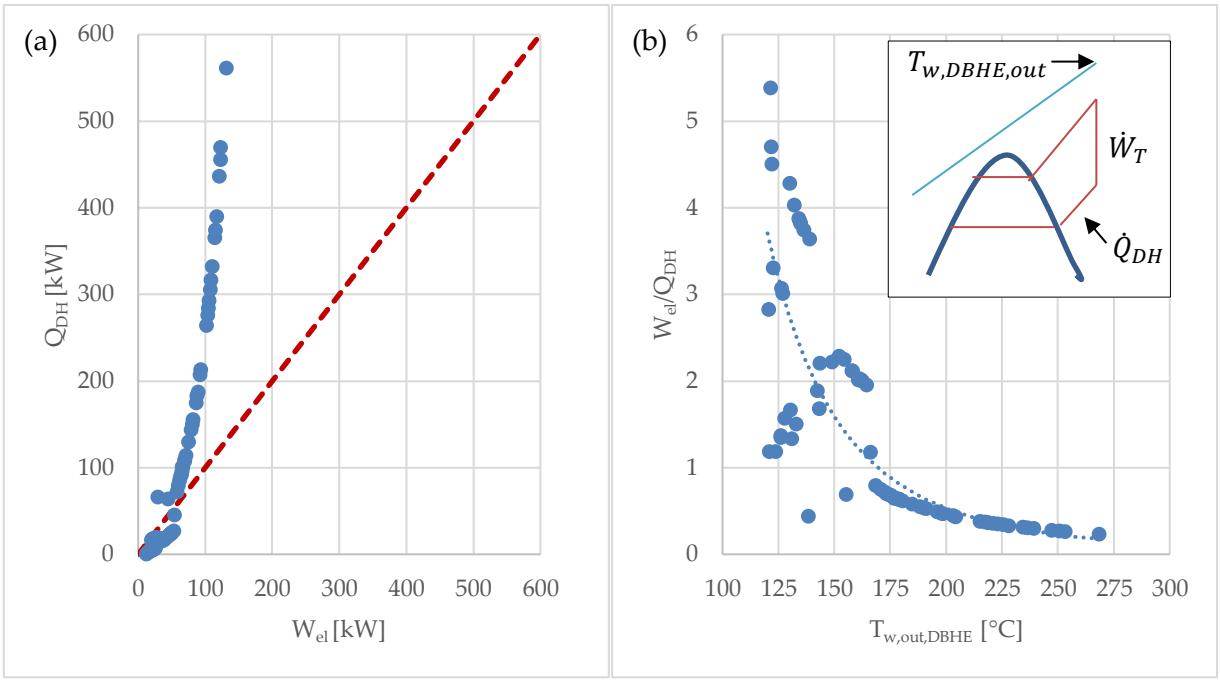

Figure 15 – (a) Thermal vs. power production in the maximum-exergy configurations for the ORC + DH utilization system; (b) Optimal ratio between power and thermal production depending on extracted temperature for ORC +DH utilization system.

4.3. Optimize the exergy efficiency or the extracted energy: what strategy?

The optimization of the exergy performance of a plant is the most correct approach by the thermodynamic point of view. Anyway, this paper concerns the use of deep borehole heat exchangers to be linked to thermal or electrical plants, so it is reasonable the research of the maximum production, too: for each combination of ground properties and user plant design variables, the code extracts the ones with maximum heat or power, and it estimates the required mass flow rate in the DBHE. The Figures 16 compare the two strategies, the exergy optimization and the production optimization, demonstrating that the clouds of data are not so far from each other, especially for the layouts composed by only one plant. Thus, a strategy based on the optimization of exergy efficiency may guarantee also the maximum production, although an ad hoc study on the real performance of the plant must be carried out.

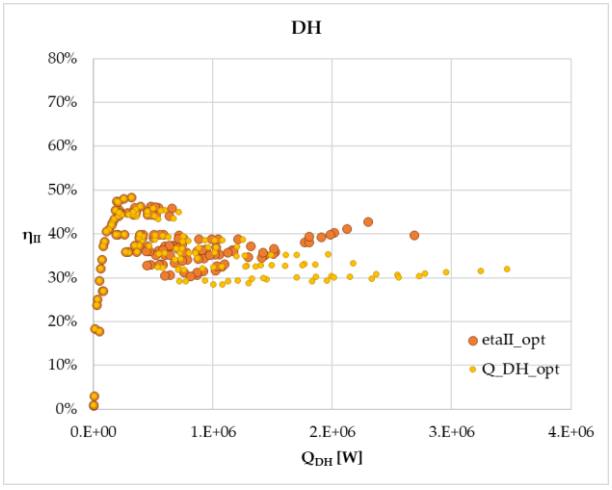

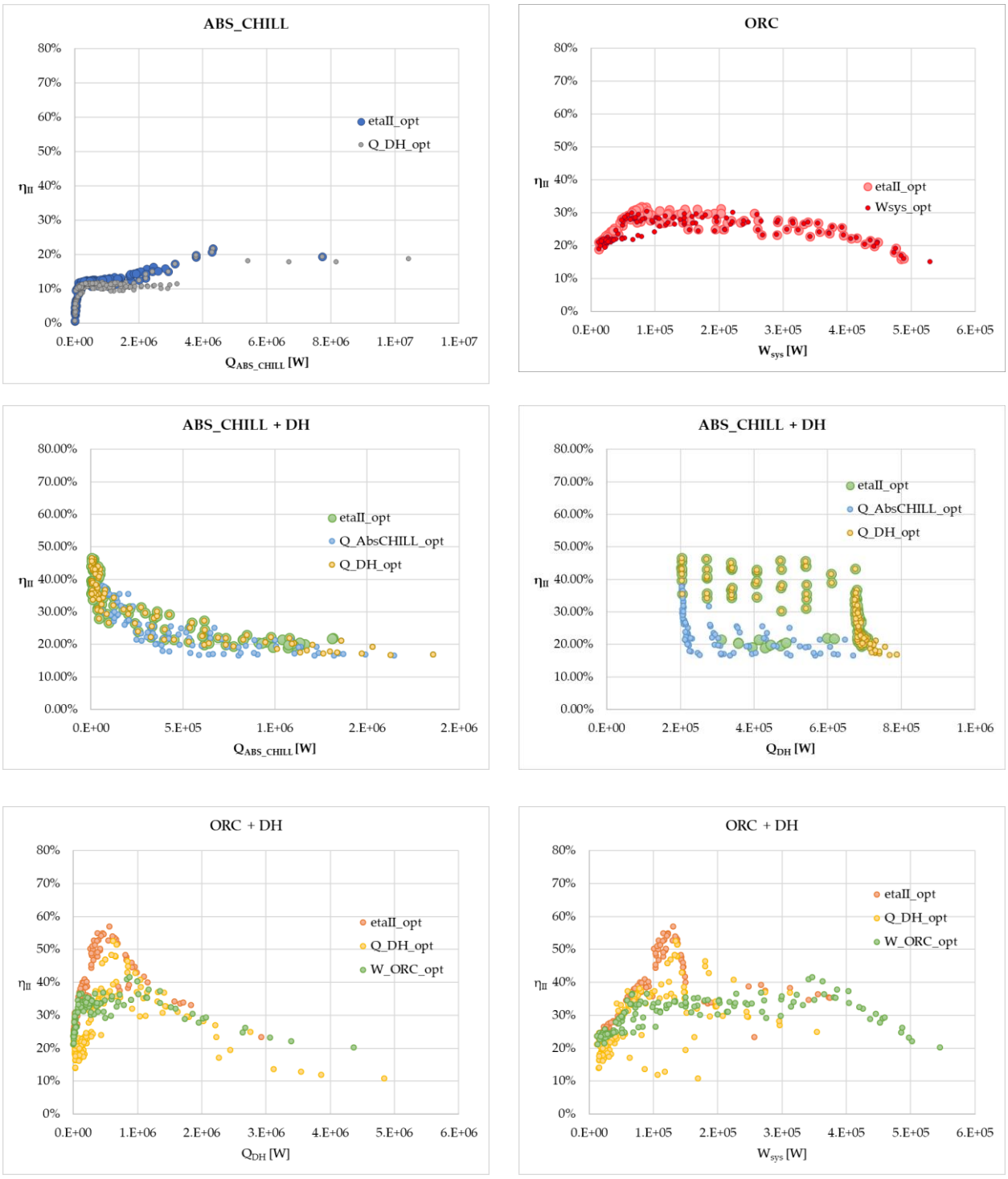

Figure 16 – Production vs exergy efficiency: comparison of exergy optimization and production optimization.

Figure 17 investigate what is the plant to boost to maximize the exergy efficiency in the proposed combined layouts (ABS_CHILL + DH and ORC + DH) with optimized heat and power production. The results indicate that the heat produced by the DH plant is the final use to be maximized to maintain the maximum (possible) values of η_{II} for the ABS_CHILL + DH layout. For the ORC + DH layout, it is recommended to improve the electrical production until the ground temperature reaches the value of 350 °C.

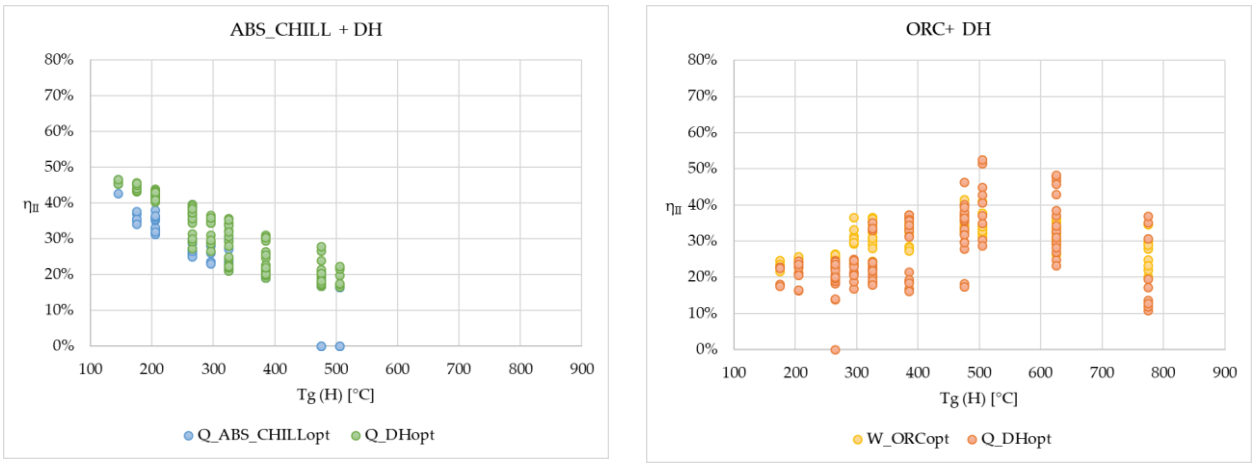

Figure 17 – Relation between temperature and exergy efficiency for each plant composing the combined layouts.

5. Conclusions

The target of this paper is to propose a fast method to evaluate the best use of deep borehole heat exchangers to exploit geothermal resources. Although the interest for this technology and the number of scientific works on the topic is increased a lot in the last 10 years, the authors are still divided regarding the best final use of the extracted heat. This uncertainty is probably due to the wide ranges of depth wells, geothermal resources and ground properties, that determine the feasibility of a direct use plant or a power plant.

In this work, we have evaluated five possible utilization strategies of DBHE technology. To discuss the layouts, the exergy efficiency has been chosen as the main performance index as it allows the comparison of heating, cooling and power production on a homogeneous base. A sensitivity analysis involving 225 well depth, geothermal source temperature, and ground thermo-physical properties has been performed to analyze the exergy efficiency of considered user systems in different contexts. For each configuration, the main operative parameters (i.e., DBHE flow rate and the inlet temperature) have been optimized to achieve the highest exergy efficiency.

The results have shown a good potential of district heating application when the geothermal source temperature is between 100 ÷ 300 °C, indeed DH ensures the highest values of both useful energy and exergy efficiency. The absorption chiller alone does not result in good performances as the energy conversion device has a too low exergy efficiency. Power production through ORC technology shows performances similar to the typical values of geothermal binary plants. However, the amount of the produced electricity is limited by the low energy efficiency of the power plant and by the exergy losses at the de-superheating and condensing section. Therefore, the amount of useful exergy is lower than the one produced by the thermal configurations, though the greater exergy value of the electrical power. The coupling of power production and downstream DH technology is the best solution for geothermal source temperature above 300 °C as it combines the electricity production and minor exergy losses at the bottom pressure of the ORC cycle.

Additionally, in this work, we presented preliminary design tools to obtain first-attempt values and the optimal trends of the main design variables for each of the five possible utilization. For an application involving the ORC power plant, the maximum-exergy design strategy corresponds to

maximize the outlet temperature from the DBHE and the evaporation temperature of the working cycle. Therefore, low DBHE flow rates and high inlet temperatures should be used. For thermal applications involving DH technologies, dimensionless maps showing the optimal inlet temperature as a function of the ground temperature profile have been proposed. Besides, the optimal flow rate can be estimated through the proposed NTU maps.

Future developments of the present work involve the analysis of other end-user applications and system layouts. Additionally, other fluids and power cycles should be investigated to properly exploit configurations with wellhead fluid temperature greater than 300 °C in replacement of isobutane.

References

Akbulut U, Utlu Z, Kincay O: Exergoenvironmental and exergoeconomic analyses of a vertical type ground source heat pump integrated wall cooling system. Appl. Therm. Eng. 102 (2016) 904–921

Akhmadullin I, Tyagi M: Design and analysis of electric power production unit for low enthalpy geothermal reservoir applications. World Academy of Science, Engineering and Technology, International Journal of Environmental, Chemical, Ecological, Geological and Geophysical Engineering, Vol: 8, No: 6, 2014

Akpinara EK, Hepbasli A: A comparative study on exergetic assessment of two ground-source (geothermal) heat pump systems for residential applications. Building and Environment 42 (2007) 2004–2013

Al-Mousawi FN, Al-Dadah R, Mahmoud S: Integrated adsorption-ORC system: comparative study of four scenarios to generate cooling and power simultaneously. Appl. Therm. Eng. 114, 2017, 1038-1052.

Alimonti C, Conti P, Soldo E: A comprehensive exergy evaluation of a deep borehole heat exchanger coupled with a ORC plant: the case study of Campi Flegrei. Energy, 189, 15 December 2019, 116100

Alimonti C, Soldo E: Study of geothermal power generation from a very deep oil well with a wellbore heat exchanger. Renewable Energy 2016, 86: 292-301

Alimonti C, Soldo E, Berardi D, Bocchetti D: A comparison between energy conversion systems for a power plant in Campi Flegrei geothermal district based on a WellBore Heat eXchanger. Proceedings of European Geothermal Congress 2016 – Strasbourg (France) – 19-23 September 2016

Ally MR, Munk JD, Baxter VD, Gehl AC: Exergy analysis of a two-stage ground source heat pump with a vertical bore for residential space conditioning under simulated occupancy. Appl. Energy 155 (2015) 502–514

Ambriz-Díaz VM, Rubio-Maya C, Ruiz-Casanova E, Martínez-Patiño J, Pastor-Martínez E: Advanced exergy and exergoeconomic analysis for a polygeneration plant operating in geothermal cascade. Energy Conversion and Management 203 (2020) 112227

Baccoli R, Mastino C, Rodriguez G: Energy and exergy analysis of a geothermal heat pump air conditioning system. Applied Thermal Engineering 86 (2015) 333 - 347

Barbacki A: Classification of geothermal resources in Poland by exergy analysis—Comparative study. Renewable and Sustainable Energy Reviews 16 (2012) 123– 128

Bejan A, Tsatsaronis G, Moran M: Thermal design and optimization. Wiley, New York (1996).

Bi Y, Wang X, Liu Y, Zhang H, Chen L: Comprehensive exergy analysis of aground-source heat pump system for both building heating and cooling modes. Appl. Energy 86 (2009) 2560–2565.

Caulk RA and Tomac I: Reuse of abandoned oil and gas wells for geothermal energy production. Renewable Energy 112 (2017) 388-397.

Casarosa C, Conti P, Franco A, Grassi W, Testi D. Analysis of thermodynamic losses in ground source heat pumps and their influence on overall system performance. J Phys Conf Ser 547 (2014) #012006

Conti P: Dimensionless maps for the validity of analytical ground heat transfer models for GSHP applications. Energies 9 (2016) #890

Conti P, Testi D, Grassi W: Revised heat transfer modeling of double-U vertical ground-coupled heat exchangers. Appl Therm Eng 106 (2016) 1257–1267.

Davis AP, Michaelides EE: Geothermal power production from abandoned oil wells. Energy 2009, 34: 866-872

DiPippo R, (2004). Second law assessment of binary generating power from low-temperature geothermal fluids. Geothermics 33, 565–586

Ehyaei MA, Ahmadi A, El Haj Assad M, Rosen MA: Investigation of an integrated system combining an Organic Rankine Cycle and absorption chiller driven by geothermal energy: Energy, exergy, and economic analyses and optimization. Journal of Cleaner Production 258 (2020) 120780.

Erbay Z, Hepbasli A: Application of conventional and advanced exergy analyses to evaluate the performance of a ground-source heat pump (GSHP) dryer used in food drying. Energy Convers. Manage 78 (2014) 499–507

Fallah M, Akbarpour Ghiasi R, Hasani Mokarram N: A comprehensive comparison among different types of geothermal plants from exergy and thermoeconomic points of view. Thermal Science and Engineering Progress 5 (2018) 15–24

Feng Y, Tyagi M, White CD: A downhole heat exchanger for horizontal wells in low-enthalpy geopressured geothermal brine reservoirs. Geothermics 2015, 53: 368-378

Fiaschi D, Manfrida G, Rogai E, Talluri L: Exergoeconomic analysis and comparison between ORC and Kalina cycles to exploit low and medium-high temperature heat from two different geothermal sites. Energy Conversion and Management 154 (2017) 503–516

Gehringer M and Loksha V (2012). Geothermal Handbook: Planning and Financing Power Generation. ESMAP technical report; no. 002/12. World Bank, Washington, DC. © World Bank

Galoppi G, Biliotti D, Ferrara G, Carnevale EA, Ferrari L: Feasibility study of a geothermal power plant with a double-pipe heat exchanger. Energy Procedia 2015, 81: 193-204

Ganjehsarabi H, Gungor A, Dincer I: Exergetic performance analysis of Dora II geothermal power plant in Turkey. Energy 46 (2012) 101-108.

Gökgedik H, Yürüsoy M, Keçebas A: Improvement potential of a real geothermal power plant using advanced exergy analysis. Energy 112 (2016) 254-263.

Hepbasli A: Thermodynamic analysis of a ground-source heat pump system for district heating. International Journal of Energy Research 29 (2005) 671–687

Hu P, Hu Q, Lin Y, Yang W, Xing L: Energy and exergy analysis of a ground source heat pump system for a public building in Wuhan, China under different control strategies. Energy and Buildings 152 (2017) 301–312

Kang S, Li H, Liu L, Lei J, Zhang G: Exergy analysis of a novel CHP–GSHP coupling system. Appl. Therm. Eng. 93 (2016) 308–314

Kizilkan O, Dincer I: Exergy analysis of borehole thermal energy storage system for building cooling applications. Energy and Buildings 49 (2012) 568–574

Kohl T, Brenni R, Eugster W: System performance of a deep borehole heat exchanger. Geothermics 2002, 31: 687-708

Kotas TJ: The exergy method of thermal plant analysis. Krieger Publishing Company, Malabar (FL), 1995

Kujawa T, Nowak W, Stachel AA: Utilization of existing deep geological wells for acquisitions of geothermal energy. Energy 2006, 31: 650-664

IRENA (2019), Renewable capacity statistics 2019, International Renewable Energy Agency (IRENA), Abu Dhabi. ISBN 978-92-9260-123-2 (PDF)

Lavine AS, DeWitt DP, Bergman TL, Incropera FP: Fundamentals of heat and mass transfer. 7th John Wiley & Sons Inc, Hoboken (NJ) (2011)

Le Lous M, Larroque F, Dupuy A, Moignard A: Thermal performance of a deep borehole heat exchanger: Insights from a synthetic coupled heat and flow model. Geothermics 2015, 57: 157–172

Lee KC: Classification of geothermal resources by exergy. Geothermics 30 (2001), 431-442

Leveni M, Manfrida G, Cozzolino R, Mendecka B: Energy and exergy analysis of cold and power production from the geothermal reservoir of Torre Alfina. Energy 180 (2019) 807-818

Li R, Ookab R, Shukuya M: Theoretical analysis on ground source heat pump and air source heatpump systems by the concepts of cool and warm exergy. Energy and Buildings 75 (2014) 447–455

Tailu Li T, Xu Y, Wang J, Kong X, Zhu J: Poly-generation energy system driven by associated geothermal water for oilfield in high water cut stage: A theoretical study. Geothermics 76 (2018) 242–252

Macenić M and Kurevija T: Revitalization of abandoned oil and gas wells for a geothermal heat exploitation by means of closed circulation: Case study of the deep dry well Pčelić-1. Interpretation, 6(1), 1-9, (2018).

Mokhtari H, Hadiannasab H, Mostafavi M, Ahmadibeni A: Determination of optimum geothermal Rankine cycle parameters utilizing coaxial heat exchanger. Energy 2016, 102: 260-275

Morita K, Bollmeier WS, Mizogami H (1992). An experiment to prove the concept of the downhole coaxial heat exchanger (DCHE) in Hawaii. Trans. Geotherm. Res. Council, 16, 9-16

Mottaghy D, Dijkshoorn L: Implementing an effective finite difference formulation for borehole heat exchangers into a heat and mass transport code. Renewable Energy 45 (2012) 59-71.

Nalla G, Shook GM, Mines GL, Bloomfield KK: Parametric sensitivity study of operating and design variables in wellbore heat exchangers. Geothermics 2005, 34: 330–346

NIST standard reference database 23: reference fluid thermodynamic and transport properties-REFPROP, version 9.1, National Institute of Standards and Technology, Standard Reference Data Program, Gaithersburg, Maryland (2013)

Noorollahi Y, Pourarshad M, Jalilinasrabady S, Yousefi H: Numerical simulation of power production from abandoned oil wells in Ahwaz oil field in southern Iran. Geothermics 2015, 55: 16-23

Ozgener O, Hepbasli A: Exergoeconomic analysis of a solar assisted ground-source heat pump greenhouse heating system. Appl. Therm. Eng. 25 (2005) 1459–1471

Ozgener L, Hepbasli A, Dincer I, (2004). Thermo-mechanical exergy analysis of Balcova geothermal district heating system in Izmir, Turkey. ASME J. Energy Resour. Technol. 126, 293–301

Ozgener L, Hepbasli A, Dincer I: Energy and exergy analysis of Salihli geothermal district heating system in Manisa, Turkey. Int. J. Energy Res. 2005; 29:393–408

Ozgener L, Hepbasli A, Dincer I: Energy and exergy analysis of the Gonen geothermal district heating system, Turkey. Geothermics 34 (2005) 632–645

Ramajo H, Tritlla J, Levresse G, Tello-Hinojosa E, Ramírez G, and Pérez H: New SExI tools to evaluate the evolution and anthropic disturbance ingeothermal fields: The case of Los Azufres geothermal field, México. Revista Mexicana de Ciencias Geológicas, 27, 3, 2010, p. 520-529

Renaud T, Verdin P, Falcone G (2019). Numerical simulation of a Deep Borehole Heat Exchanger in the Krafla geothermal system. Int. J. Heat Mass Transfer, 143, 118496, DOI: 10.1016/j.ijheatmasstransfer.2019.118496)

Rosen MA, Dincer I: Exergy: Energy, Environment and Sustainable Development. 2nd ed. Elsevier; (2013)

Stefansson V: World Geothermal Assessment. Proceedings World Geothermal Congress 2005 Antalya, Turkey, 24-29 April 2005

Taleghani AD: An improved closed-loop heat extraction method for geothermal resources. Journal of Energy resources Technology, ASME, December 2013, 135 (4), doi: 10.1115/1.4023175

Templeton JD, Ghoreishi-Madiseh SA, Hassani F, Al-Khawaja MJ: Abandoned petroleum wells as sustainable sources of geothermal. Energy 2014, 70: 366–373

UNEP. Sustainable Building Policies in Developing Countries (SPOD). <http://www.unep.org/sbci/pdfs/SPOD%202-pager_english.pdf>; 2014 [22.08.16]

Wang Z, Wang F, Liu J, Ma Z, Han E, Song M: Field test and numerical investigation on the heat transfer characteristics and optimal design of the heat exchangers of a deep borehole ground source heat pump system. Energy Conversion and Management 153 (2017) 603–615

Wang Z, McClure MW, Horne RN: A single-well EGS configuration using a thermosiphon. Proceedings of Thirty-Fourth Workshop on Geothermal Reservoir Engineering Stanford University, Stanford, California, February 9-11, 2009

Wight NM, Bennett NS: Geothermal energy from abandoned oil and gas wells using water in combination with a closed wellbore. Applied Thermal Energy 2015, 89: 908-915

Yari M: Exergetic analysis of various types of geothermal power plants. Renewable Energy 35 (2010) 112–121

Acknowledgements

The authors declare that they have no competing interests.

The authors declare that no other contributors have provided technical or writing assistance.